DOI: 10.1002/ejoc.200700926

Development of Bis(2-picolyl)amine–Zinc Chelates for Imidazole Receptors

Taina Routasalo,[a] Juho Helaja,[a] Jari Kavakka,[b] and Ari M. P. Koskinen*[a]

Keywords: Amines / N,O ligands / Heterocycles / Zinc / Chelation

New phenyl and phenol bis(2-picolyl)amine (Dpa) derivatives have been synthesized in order to generate zinc chelates for imidazole anion receptors. Previously, binuclear phenolic zinc and copper chelates have shown affinity for pyrophosphate and guanidine anions, respectively. Herein we report significant imidazole affinity increasing from 2.38×10^6 to 2.90×10^7 for phenol-bridged binuclear zinc–Dpa chelates, as evidenced by dynamic and titration ^{1}H NMR studies. Among the Dpa chelates investigated, the zinc-coordinated phenol group plays a crucial role in the mechanism of anion binding. Low-temperature ^{1}H NMR experiments suggest a σ_v-symmetric geometry for the imidazole chelate. Computational DFT studies at the B3LYP level of theory imply that imidazole binding displaces the phenol bridge between the zinc ions.

Introduction

The development of anion receptors is a major current challenge in the field of supramolecular chemistry. Anion recognition can be achieved through a variety of molecular interactions: Electrostatic interactions, hydrogen bonds, hydrophobic effects, and metal or Lewis acid coordination, or combinations of these interactions working together.[1] Among these interactions, metal coordination offers a rational approach to the design and construction of self-correcting assemblies with a wide range of accessible geometries.[2] The concept of metal-templated self-assembly in receptor design has been inspired by various biological systems in which proteins act as self-assembling binding sites.[3] Among the metalloproteins, zinc enzymes offer a large number of coordination motifs and thus provide models for the design of zinc-based anion receptors.[4] Our model for imidazole receptor design was the enzyme superoxide dismutase (SOD), which has a bimetallic Zn,Cu imidazole bridging moiety.[5] Previously, self-assembling and ion-specific ligands for Zn and Cu ions had been developed based on SOD mimicry.[6] We took the Zn,Cu-bridged histidine residue of the SOD enzyme as a model for the design of an imidazole anion-binding receptor. We further envisioned that an appropriately chelated metal ion-pair would be able to contribute to imidazole anion binding in the same manner as the bimetallic cation-pair does in the SOD enzyme.

Anion recognition with bimetallic coordination complexes has been reviewed recently.[7] For this purpose bis(2-picolyl)amines (Dpa) **1** (Figure 1) are well-known tridentate ligands capable of donating three electron pairs to a cationic metal center.[8–10] The Dpa geometry and its conformational flexibility gives this ligand a strong affinity for biologically interesting Zn^{2+} and Cu^{2+} ions, whereas tridentate amine–metal chelation leaves basic coordination places free for counterions. Accordingly, Dpa ligands have been used as such,[11] but more widely as linked ligand units in larger host structures.[12,13] Recently, examples of Dpa-functionalized metal–anion fluorescence probes have been reported in which Dpa units have been linked to a fluorescent host molecule.[13b,14–16] Lately, it has also been demonstrated that bimetallic double Dpa chelates can function in molecular recognition of anionic species, for example, phosphate,[17] pyrophosphate,[18] or phospholipid[19] anions, as well as histidine residues to some extent.[20]

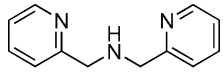

1

Figure 1. Bis(2-picolyl)amine (Dpa).

We have studied metal–ligand structures that are capable of zinc chelation and usable for anion recognition purposes in biological environments. The imidazole binding sites previously reported have been mainly bimetallic imidazole cryptand structures, including the recent work of Fabbrizzi et al. in which fluorescent chemosensing activity was reported for imidazole binding.[21] Regiospecific protein-surface sensing is highly desirable in many biotechnological and pharmaceutical processes, for example, in protein detection and for analyzing enzyme activation or deactivation.

[a] Department of Chemistry, Helsinki University of Technology, P. O. Box 6100, 02015 HUT, Finland
E-mail: ari.koskinen@tkk.fi
[b] Laboratory of Organic Chemistry, Department of Chemistry, University of Helsinki,
A. I. Virtasen aukio 1, P. O. Box 55, 00014, Finland

Supporting information for this article is available on the WWW under http://www.eurjoc.org or from the author.

Our ultimate goal is to construct chelates capable of histidine residue recognition in proteins that will act as chemical sensors. Dpa-based chelates form a promising tool with potential applications both in metal-cation chelation and subsequent chelate-based anion recognition. Herein we report the synthesis of new Dpa chelators and the ability of their zinc chelates to act as imidazole anion receptors. The recognition event has been studied by ^{1}H NMR and molecular modeling techniques.

Results and Discussion

We have constructed Dpa ligands based on three different skeleta: A monosubstituted compound **2a** and disubstituted compounds **2b** and **2c**–**e**. All the Dpa ligands have a potentially linkable R group (H, CO_2Me or NO_2) (Figure 2). In the disubstituted ligand **2c**, the phenolic oxygen between the two ligands is capable of forming a bridge between two metal ions (**3**, Figure 3). Such bimetallic chelates have been shown to participate in anion recognition.[20,21] Dapporto and co-workers have developed dinuclear Zn or Cu amino-phenolic ligands for small anionic molecules.[22] Unlike Fusi and co-workers, we used the pyridine nitrogen atoms in structures **2c**, **2d**, and **2e** for metal coordination instead of primary amines.

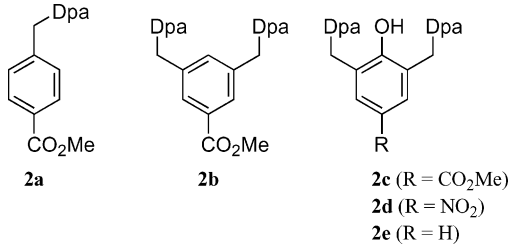

Figure 2. Dpa ligands based on different skeleta **2a**–**2e**.

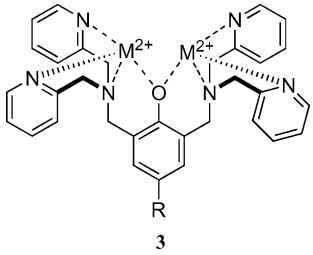

Figure 3. Phenol-bridged structure between two metal ions.

Synthesis

The monosubstituted ligand **2a** was prepared as shown in Scheme 1. Wohl–Ziegler bromination occurs under neutral conditions with *N*-bromosuccinimide (NBS) and a catalytic amount of 2,2′-azobis(isobutyronitrile) (AIBN) as initiator.[23] The brominated molecule was then substituted with the Dpa ligand under basic conditions.

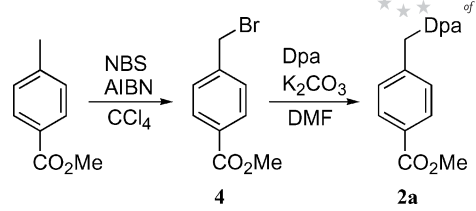

Scheme 1. Synthesis of the monosubstituted chelator **2a**.

The disubstituted ligand **2b** was prepared in the same manner as ligand **2a** by Wohl–Ziegler bromination and substitution with Dpa (Scheme 2).

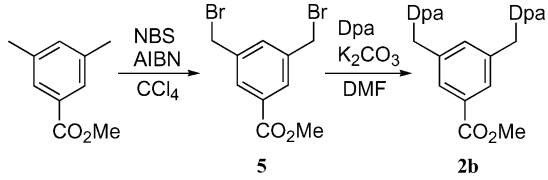

Scheme 2. Synthesis of the disubstituted chelator **2b**.

Disubstituted phenolic ligands **2c**–**e** were synthesized by three different routes (Schemes 3, 4, and 5). The *para*-ester skeleton **2c** was synthesized starting from methyl 4-hydroxybenzoate, which was diformylated with hexamethylenetetramine in TFA by using a modified Duff reaction.[24] The product **6** precipitated in 87% yield after stirring (2–4 h) in a large excess of water. The formyl substituents were

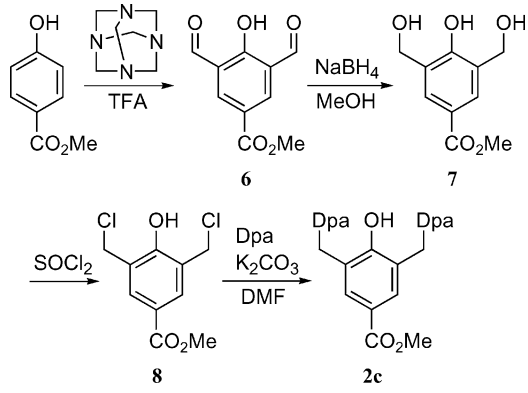

Scheme 3. Synthesis of the disubstituted chelator **2c**.

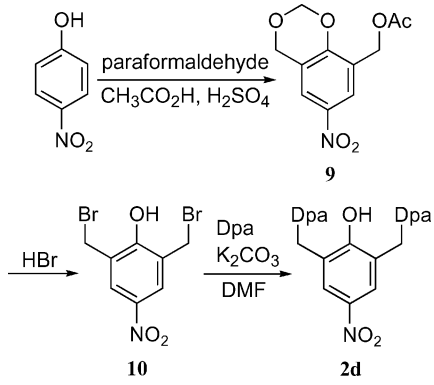

Scheme 4. Synthesis of the disubstituted chelator **2d**.

reduced with $NaBH_4$[25] and the primary alcohols were selectively converted into chlorides with $SOCl_2$.[26] Final substitution with Dpa was performed as described above.

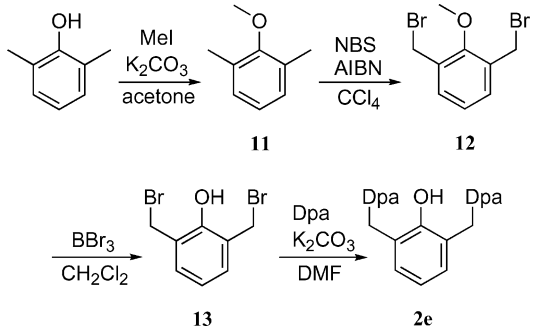

Scheme 5. Synthesis of the disubstituted chelator **2e**.

In the synthesis of the nitro-substituted ligand **2d** (Scheme 4), the benzodioxine derivative was obtained from *p*-nitrophenol by using paraformaldehyde under acidic conditions.[27] The temperature must be carefully controlled in order to obtain good yields of dioxine **9**: Even a small deviation of a few degrees from the optimal +60 °C led to the domination of side-products. Dioxine **9** was brominated in refluxing HBr to give compound **10**. Subsequently, the bromines were substituted with Dpa ligands to obtain **2d**.

The synthesis of ligand **2e** was similar to that of ligands **2a** and **2b**, that is, by Wohl–Ziegler bromination and substitution with Dpa (Scheme 5). The phenolic OH was protected as the methyl ether before the radical reaction and subsequently deprotected with BBr_3.

Despite the similarities of the ligands, it was found that general synthetic methods could not be applied to all the ligand syntheses: For example the successful diformylation of *para*-phenol ester **2c** and the dioxine route to **2d** gave only negligible yields with other ligands. The overall yields for the syntheses of **2a**–**e** varied from 17 to 48%. Finally, the most laborious part of the syntheses was the chromatographic purification, which suffered from low capacity and concentration-dependent retention times that were characteristic of all the Dpa ligands.

Imidazole Dpa–Zinc Receptors: Geometry and Strength

We studied the coordination of imidazole to the zinc chelates by variable-temperature (dynamic) and titration ^1H NMR techniques. The coordination geometry and strength were further examined by molecular modeling using DFT.

^1H NMR Titration Measurements

The characteristic coordination-dependent magnetic behavior of imidazole protons allowed us to determine, based on molecular symmetry, whether imidazole exhibits a mono- or bidentate coordination to zinc ions. In the monodentate case, imidazole would have a chemically nonequivalent magnetic environment for the δ^1 protons. Consequently, the signals would be split, whereas in the bidentate case only one signal would be detected due to a higher molecular symmetry (Figure 4).

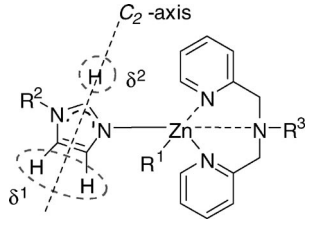

Figure 4. Determination of the coordination geometry by analysis of the ^1H NMR shifts of the imidazole. The red broken line illustrates the C_2 symmetry axis of the imidazole.

All the studied imidazole–zinc chelates exhibited symmetric behavior at 30 °C, that is, only one signal was observed for the δ^1 protons, as listed in Table 1. However, this could be attributed to rapid chemical exchange at this temperature.

Table 1. ^1H NMR chemical shifts [ppm] of imidazole with different chelates measured in CD_3OD.

Chelate system	δ^1	δ^2	$\Delta\delta^1$	$\Delta\delta^2$
Imidazole	7.05	7.67		
Imidazole + $Zn(NO_3)_2$	7.28	8.06	0.23	0.39
2a + $Zn(NO_3)_2$ + imidazole	7.29	8.16	0.24	0.49
2b + $Zn(NO_3)_2$ + imidazole	7.37	8.36	0.32	0.69
2c + $Zn(NO_3)_2$ + imidazole	7.52	8.76	0.47	1.09
2d + $Zn(NO_3)_2$ + imidazole	7.53	8.77	0.48	1.10
2e + $Zn(NO_3)_2$ + imidazole	7.46	8.60	0.41	0.93

The imidazole signals could be recognized in all cases, even at low concentrations at room temperature. Thus, the **2a**–**e** zinc chelates were titrated against imidazole to determine the strength of the coordination (Figures 5 and 6). Ligand **2a** shows a low affinity for imidazole, as indicated by its steeply descending curve. The curve obtained with ligand **2b** indicates that the imidazole binds this zinc chelate with a slightly improved affinity compared with that of **2a**.

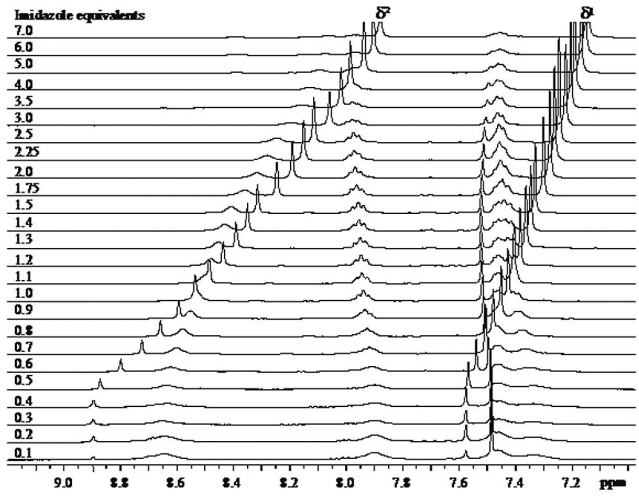

Figure 5. ^1H NMR spectra of **2c** + 2 equiv. $Zn(NO_3)_2$ titrated against imidazole (in CD_3OD).

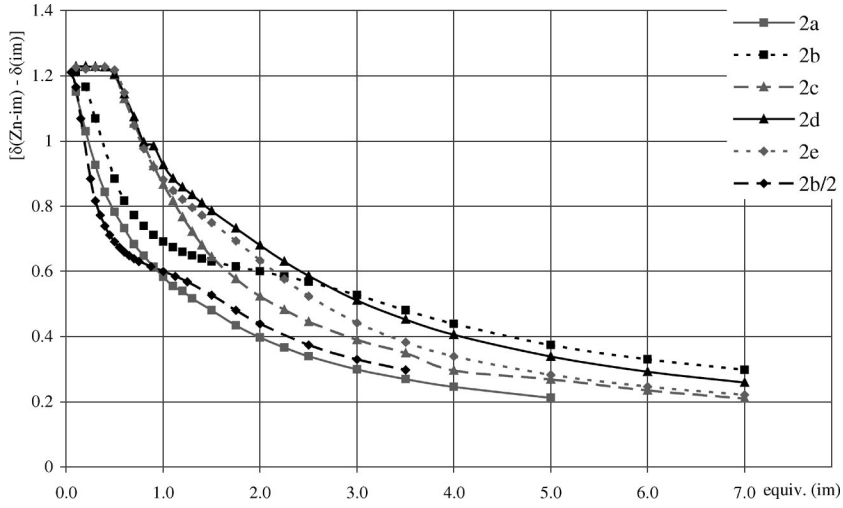

Figure 6. Imidazole titration curves for the **2a**–**e** zinc chelates. The *y* axis represents the difference between the δ^2 value of the chelated and the free imidazole: $\Delta\delta^2 = [\delta^2(\text{Zn–imidazole–}\mathbf{2}\text{ chelate}) - \delta^2(\text{imidazole})]$. The curve **2b**/2 represents **2b** in which the imidazole equiv. number is calculated with respect to the number of Dpa units.

However, when the same comparison was performed taking into account the number of Dpa units per ligand, that is, **2a** and **2b**/2 curves, the result is that **2b** is a weaker imidazole binder than **2a** below the concentration of 1 equiv. imidazole (Dpa). This can be attributed to the stronger intermolecular chelation of **2a** relative to the intramolecular chelation of **2b**. The steeper slope of **2b**/2 before the addition of 1 molar equiv. (per Dpa unit) can be attributed to entropic factors, that is, after saturation of the zinc–Dpa chelates with imidazole the intramolecular ligand exchange becomes visible.

For phenol chelates **2c**, **2d**, and **2e**, the imidazole titration curves indicate significant binding activity. In these cases the imidazole $\Delta\delta^2$ value was unaffected until after more than 0.4–0.6 equiv. imidazole had been added to the solution (Figure 6). After 1.0 equiv. of imidazole had been added, the shapes of the curves for these chelates differed somewhat, which can be attributed to solubility effects. Nevertheless, the chelate with **2d** exhibits the slowest descent, which indicates the strongest affinity.

The coordination strength can also be determined by inspecting the chemical shifts of the imidazole protons: In strong imidazole–zinc coordination, the nitrogen electron-donation is expected to make the imidazole ring electron-deficient and thereby cause deshielding and downfield shifts of the imidazole protons. The results correlate well with the titration results: Phenolic chelates **2c**–**e** are strongly deshielded with *p*-nitrophenol **2d** chelated imidazole the most affected, as shown by comparison of the $\Delta\delta^1$ and $\Delta\delta^2$ values (Table 1). The fact that the δ values for the chelate of **2b** are less deshielded indicates that weaker imidazole chelation occurs for this chelate. However, the values are still significantly more deshielded than those of the mono-Dpa chelate **2a**, which suggests a cooperative role for the zinc ions in the chelation.

To confirm the results described above, the binding constants (K_A) for chelates **2b**–**e** were calculated. Imidazole (S_0 = amount of substrate) was titrated against zinc–ligand (R_0 = amount of receptor) and the chemical shift of imidazole's δ^2 proton (Figure 4) was plotted versus the quantity of the zinc receptor. The results (Table 2) were analyzed by using Equation (1)[28] on the assumption that one binding constant could explain the observed binding phenomena.[29] The binding constants show that **2d** has the strongest coordination strength, whereas **2b** has a substantially weaker chelation capability compared with chelates **2c**–**e** [Equation (2)].

$$\delta_{obs} = \delta_s + \Delta\delta/2S_0\{K_D + S_0 + R_0 - [(K_D + R_0 + S_0)^2 - 4R_0S_0]^{1/2}\} \quad (1)$$

$$K_A = 1/K_D \quad (2)$$

Table 2. Binding constants for **2b**–**e** zinc chelates.[a]

Chelate	K_α [1/M]
2b	2.38×10^6
2c	1.38×10^7
2d	2.90×10^7
2e	1.60×10^7

[a] The detailed procedure for determining the binding constants is described in the Supporting Information.

^{1}H NMR Variable-Temperature Measurements

The coordination geometry and strength of the imidazole–zinc(II) chelates were also explored through variable-temperature ^{1}H NMR measurements between –95 and

+30 °C (Figures 7 and 8). The distinctive feature of these measurements was that the imidazole protons formed clearly detectable singlets, even at reduced temperatures for the double Dpa **2b**–**e** chelates. This is in contrast to observations reported for amino-phenol-based chelates.[21] The singlet nature of the imidazole δ^1 values is an indication of the high molecular symmetry of these chelates and suggests bidentate imidazole coordination.

Inspection of the Dpa pyridine ^{1}H NMR chemical shifts at reduced temperatures gave information on the binding geometry and strength of imidazole. In the case of the mono-Dpa **2a**–zinc chelate, lowering the temperature caused significant signal splitting and broadening that could not be interpreted unambiguously (Figure 7). Imid-

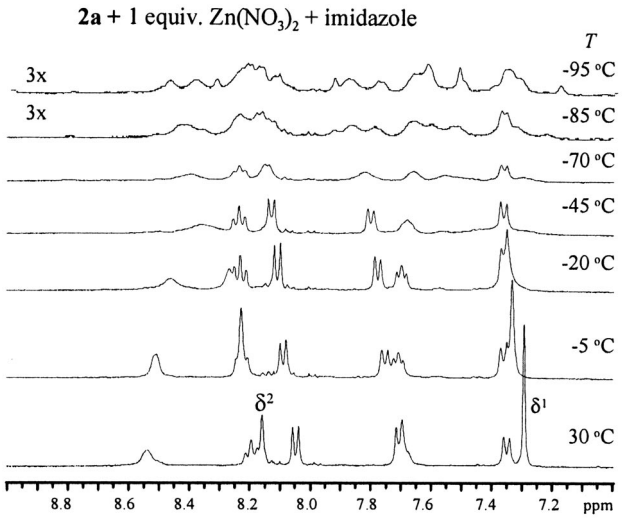

Figure 7. Variable-temperature ^{1}H NMR measurements for the **2a**–imidazole–zinc chelate.

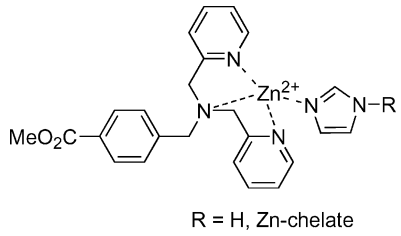

Figure 9. Imidazole coordinated through one nitrogen to the **2a**–zinc chelate (R = H) or as an anion through each nitrogen to two chelates (R = **2a**–Zn chelate).

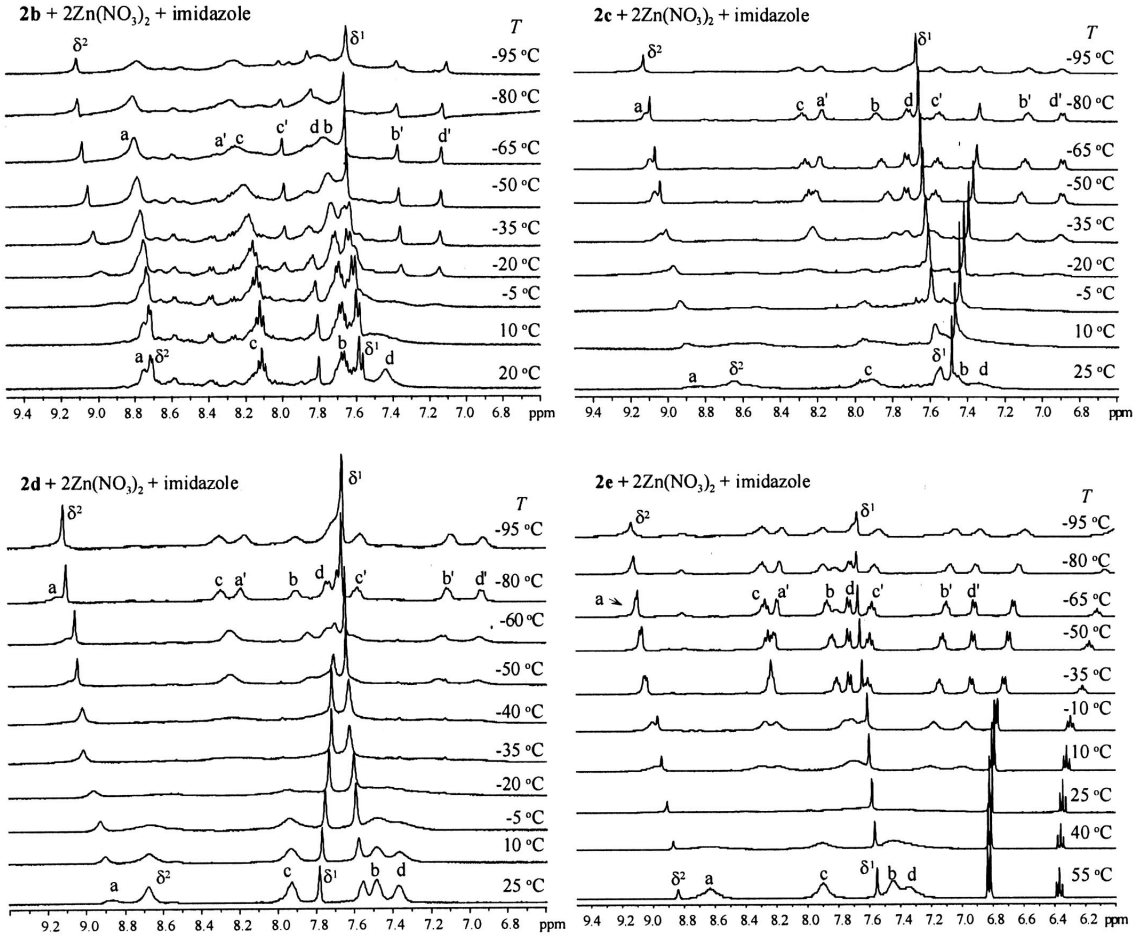

Figure 8. The aromatic regions of the variable-temperature ^{1}H NMR spectra measured for ligands **2b**–**e** with Zn and imidazole in CD_3OD. δ^1 and δ^2 denote the imidazole chemical shifts (Figure 4). The arrows and letters a–d and a′–d′ indicate pyridine protons that show splitting at reduced temperatures.

azole clearly coordinates to the zinc ions, but the degree of mono- or bidentate coordination cannot be estimated from this data (Figure 9).

The ^{1}H NMR spectra of the imidazole–zinc–**2b** chelate showed more obscure behavior at reduced temperatures than the phenolic chelates **2c**–**e**. In the case of **2b**, some chemical exchange still occurred at –70 °C. This was indicated by broad signals and an absence of correlations in the COSY spectrum. Thus, the assignment of **2b** is also partially tentative (Figure 8). The behavior is probably connected to lower chelate stability. In the case of chelate **2b**, two competing chelation models can be conspired, that is, intra- and intermolecular ones (**A** and **B**, respectively, Figure 10), both consistent with the NMR results.

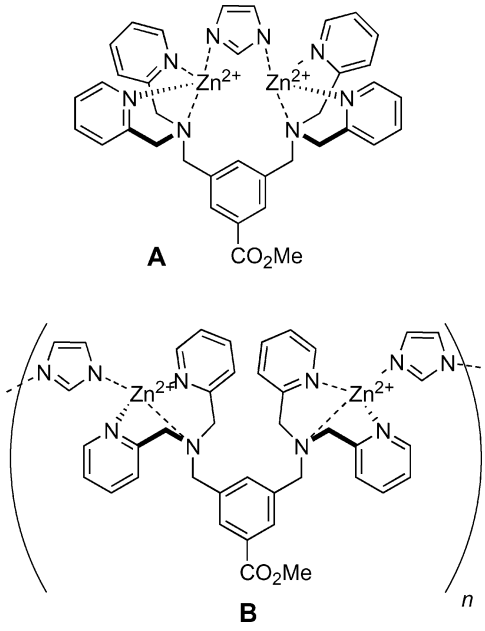

Figure 10. The imidazole–zinc–**2b** chelate could be an internal complex (**A**) or an intermolecular chelate structure (**B**).

Another feature observed in the variable-temperature measurements was a clear splitting of the pyridine proton signals, which could be detected for all phenolic chelates **2c**–**e** by lowering the temperature (Figure 8). The splitting of the pyridine signals into two major sets of signals (a–d, a′–d′) was evidenced by a COSY experiment (Figure 11). This indicates lower symmetry in the chelate: The Dpa pyridine groups experience different surroundings, which is reflected in the δ values. Two possible σ_v-symmetric geometries are illustrated in Figure 12. In variable-temperature experiments we also looked for the coalescence points of these sets of signals, which would reveal the energetics of the interconversion. Unfortunately, sharp coalescence points could not be detected in these spectra (Figure 8), but an overall trend did emerge: Signals merge upon increasing the temperature. For **2c** and **2d** this occurs between approximately –10 and +10 °C, but in both cases there is still some broadening of the signal at 25 °C. For **2e**, the coalescence point lies at around +25 °C (±10 °C), signals still being broad at 55 °C. An estimation of the related Gibbs' Free Energies (ΔG) based on the coalescence temperature using the Eyring equation gives energies of 12.0 ± 0.7 kcal/mol for **2c** and **2d**, and 13.5 ± 0.7 kcal/mol for **2e**.[30] To our surprise, the slowest chemical exchange and highest activation energies for **2c**–**e** were observed for **2e**, which has the weakest imidazole affinity according to our titration results (Figure 6). This indicates that the activation energies for conformational exchange and for complex formation are different and to some extent mutually independent.

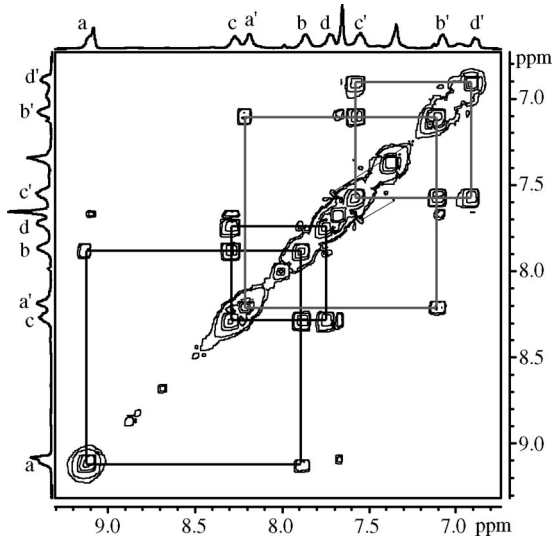

Figure 11. The aromatic part of the COSY spectrum of **2d** + 2 equiv. $Zn(NO_3)_2$ + 1 equiv. imidazole measured in CD_3OD at –70 °C. The black and gray squares depict the two clearly distinct coupling patterns for the Dpa pyridine protons a–d and a′–d′, respectively.

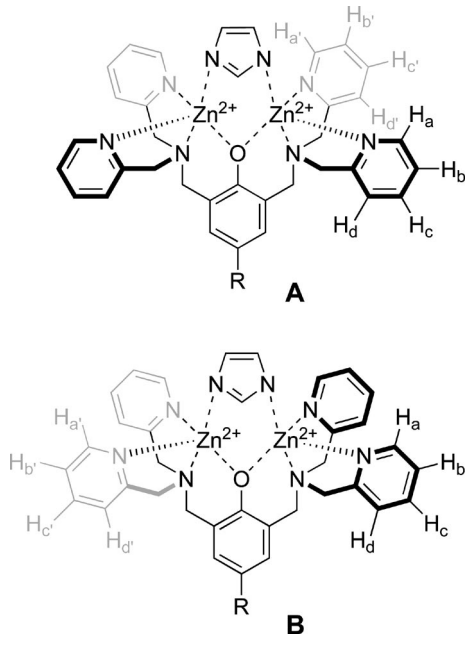

Figure 12. Two possible σ_v-symmetric geometries **A** and **B** for zinc–imidazole–**2c**–**e** chelates that can be interpreted on the basis of low-temperature ^{1}H NMR experiments.

Molecular Modeling

The imidazole binding of **2b**–**e** zinc chelates was studied computationally by carrying out DFT calculations at the B3LYP level of theory using the LACVP basis set. The primary objective of the calculations was to find theoretical evidence for the experimentally observed bidentate imidazole binding of the phenyl- and phenol-type Dpa–zinc chelates. For computational simplicity, the nitrate was replaced with a chloride ion as the counteranion.

Imidazole-bridged and -non-bridged **2b**–**e** zinc chelate geometries were computationally probed by minimizing the energy of each structure (Table 3). The starting geometry for the imidazole-bridged **2b**–zinc chelate calculation was set simply by placing the imidazole ring in between the zinc ions with bidentate nitrogen coordination. For this chelate, the calculation converged smoothly to an energy minimum at which the imidazole remained bidentate, bridging the zinc ions (Table 3, Figures 13 and 14). The imidazole nitrogen–zinc bond lengths were 2.07 and 2.18 Å in the mono- and dichloro-coordinated zinc ions, respectively. The non-bridged, that is, "opened" imidazole–**2b**–zinc chelate geometry was obtained by optimizing the monocoordinated imidazole anion as the starting geometry (Figure 14). The imidazole nitrogen–zinc ion distances were 2.03 and 5.94 Å in the coordinated and noncoordinated ions, respectively. Unexpectedly, this type of chelation geometry was energetically 2.22 kcal/mol more advantageous than the bridged, monodentate imidazole anion binding.

Table 3. Molecular modeling results for the **2b**–**e** imidazole–zinc chelates (B3LYP LACVP).

Structure	Energy [a.u.]	Relative stability of the bridge chelate ΔH (bridge-open) [kcal/mol]
2b–Zn bridge chelate	–3304.369940	–2.22
2b chelate open	–3304.373479	
2c–Zn bridge chelate	–3146.573305	4.88
2c open chelate	–3146.565529	
2d–Zn bridge chelate	–3123.198478	5.41
2d open chelate	–3123.189863	
2e–Zn bridge chelate	–2918.764323	4.10
2e open chelate	–2918.757787	

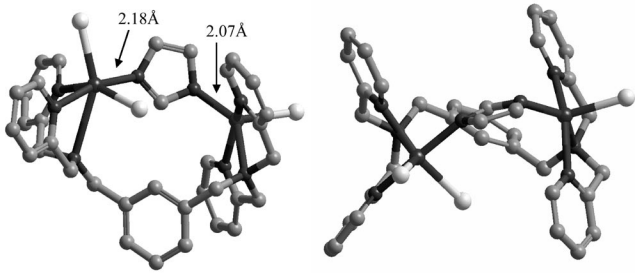

Figure 13. DFT geometry-optimized structure of **2b** + $ZnCl_2$ + ZnCl + imidazole anion chelate (side view on the left and top view on the right). The zinc ion (black) with two chlorine counter ions (white) has a distorted-octahedral anion coordination and the zinc ion with one chlorine counter ion has trigonal-bipyramidal anion coordination (hydrogen atoms have been omitted for clarity).

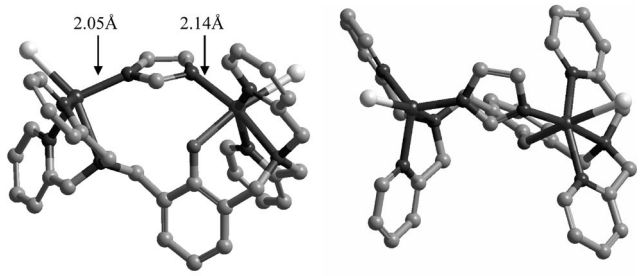

Figure 14. DFT geometry-optimized nonbridged "opened" chelate for **2e** + 2 ZnCl + imidazole anion (left) and **2b** + $ZnCl_2$ + ZnCl + imidazole anion (right).

In the case of geometry-optimized phenolic **2c**–**e** zinc chelates, the imidazole anion could not be placed between the phenolic oxygen-bridged zinc cations, but was placed next to the metals, the nitrogen atoms being located close to the bonding distance of the zinc(II) ions. The geometry optimizations that converged to the global minimum showed that the symmetric phenolic oxygen bridge between the zinc ions was opened when the imidazole anion coordinated to both of the metal ions in a bidentate manner through both of the nitrogen atoms (Figure 15). The imidazole nitrogen–zinc bond lengths were 2.14 and 2.05 Å for the phenol-coordinated and non-coordinated zinc ions, respectively. The clear energy advantage of the imidazole-bridged bidentate chelate was a somewhat surprising result as in the literature only monodentate imidazole coordination has been reported for phenol-bridged dinuclear zinc chelates.[21] We also tried to minimize the energy of the phenolic imidazole–zinc chelate structures in which one imidazole nitrogen coordinates to both zinc ions, but these were energetically less advantageous and finally converged to imidazole-bridged bidentate or "opened" structures.

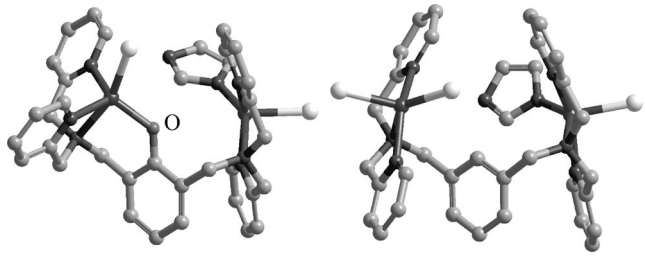

Figure 15. DFT geometry-optimized structure of **2e** + 2 ZnCl + imidazole anion chelate (side view on the left and top view on the right). In the energy-minimum structure, the imidazole anion is bridging the chelated zinc ions (black) in a bidentate manner instead of the phenol oxygen (gray).

A comparison between the open and closed systems, in which the imidazole coordinates to one or two zinc ions, respectively, is shown in Table 3. Comparison of the energies of structures **2b** and **2c** shows that the phenol group stabilizes the imidazole chelation by 7.1 kcal/mol. The general trend with respect to phenol *para* substitution is that electron-withdrawing substituents notably strengthen the imidazole chelation. The calculated difference between the unsubstituted **2e** and nitro-substituted **2d** chelate models is

1.31 kcal/mol (Table 3), whereas for CO_2Me *para*-substituted **2c** the affinity is increased by 0.78 kcal/mol relative to **2e**.

The minimum-energy structures for the phenyl and phenol chelates do not unambiguously explain the ^1H NMR differences observed at reduced temperatures, although all the calculated minima have some degree of dissymmetry with respect to the Dpa pyridine groups. The energetics imply that the chelate **2b** is looser than the phenolic chelates and thus leads to time-averaging in the NMR measurements. Moreover, inspection of the chelate **2e** geometry (Figures 14 and 15) shows that the minimum-energy structures exhibit an approximate σ_v symmetry with respect to the pyridine groups, similar to structure **A** in Figure 12.

The deviation between the *G* values estimated from the dynamic NMR measurements and from the computed enthalpies arises from the entropy, that is, the computed energies are obtained in the gas phase and in nondynamic conditions. However, as the studied systems are very similar it can reasonably be expected that the entropy factors in the systems are very similar. Hence, inspection of the relative differences is justified. Taking this into account, the experimental and theoretical relative energies correlate with high accuracy. Overall, this study shows that phenolic **2c**–**e** zinc chelates have a tendency to bind imidazole in a bidentate manner, with the electron-poor *para*-nitro zinc–**2d** chelate exhibiting the most efficient imidazole anion receptor character.

Conclusions

We have demonstrated that zinc chelates with significant affinity towards imidazole binding can be developed. The largest imidazole chelation affinity was measured for phenolic Dpa ligands in which the phenolic oxygen is known to form a bridge between two zinc ions when the imidazole is not present. The NMR and molecular modeling results show that imidazole binds in a bidentate manner to two zinc ions forming a bridge. Moreover, the modeling results imply that the imidazole bridge replaces the phenolic oxygen zinc bridge of an unbound chelate. Experimental and theoretical results also imply that the phenol chelate imidazole affinity is increased by electron-withdrawing groups *para* to the phenol group. In terms of supramolecular chemistry, novel cascade receptors for imidazole binding have been generated. The Dpa-based receptor binds cationic zinc ions, which contribute to imidazole binding.

We are currently studying the imidazole affinity of these chelates with biomaterial samples. Further Dpa ligands are also being synthesized to enable us to study whether the zinc ligands can be modified to improve their binding affinity and sensing properties.

Experimental Section

General Methods: All reagents and solvents were purchased from commercial suppliers and used without further purification with the following exceptions: DMF and THF were distilled from ninhydride and Na/benzophenone, respectively. The ^1H and ^{13}C NMR spectra were recorded at 400.133 and 100 MHz. Chemical shifts are reported in ppm using tetramethylsilane (^1H: 0 ppm) and chloroform (^{13}C: 77.0 ppm) as internal standards. Flash column chromatography was performed on Merck silica gel 60 (230–400 mesh) or on Merck aluminium oxide 90 neutral (70–120 mesh). Molecular modeling was performed with Jaguar 5.5 software via a Maestro interface 6.0 installed on a Linux 9.0 PC workstation equipped with a 3.4 GHz Pentium Intel processor and 2 GB RAM. The calculations were run for gas-phase conditions and the geometries were optimized with a DIIS algorithm using several starting geometries.

Ligand Titration Experiments: Dpa ligands **2a**–**e** were dissolved in CD_3OD (0.75 mL) in an NMR tube to obtain concentrations of 63, 43, 47, 50, and 43 mM for ligands **2a**–**e**, respectively. Thereafter the ligands were chelated with zinc by adding 1 equiv. of $Zn(NO_3)_2$ with respect to the Dpa group in each molecule. The zinc chelates formed were titrated against imidazole (2 M in MeOH).

Methyl 4-(Bromomethyl)benzoate (4): A few crystals of AIBN were added to a solution of methyl 4-methylbenzoate (6.33 g, 42.1 mmol, 100 mol-%) and NBS (7.63 g, 43.1 mmol, 102 mol-%) in CCl_4 (40 mL). The mixture was heated to 85 °C and more AIBN was added. After heating at reflux (45 min) the color of the solution changed rapidly from yellow to white and the mixture was cooled down to room temp. The solid was filtered and the solution was concentrated in vacuo. The yellow-white crude product was recrystallized from EtOAc/hexane to give 5.80 g (60%) of white crystals. R_f = 0.80 (CH_2Cl_2); m.p. 54.1–54.4 °C (ref.[31] 54–55 °C). ^1H NMR (400 MHz, $CDCl_3$): δ = 3.92 (s, 3 H), 4.50 (s, 2 H), 7.46 (d, J = 8.3 Hz, 2 H), 8.02 (d, J = 8.3 Hz, 2 H) ppm. ^{13}C NMR (400 MHz, $CDCl_3$): δ = 166.3, 164.8, 122.6, 120.9, 118.8, 52.3, 32.2 ppm.

Methyl 3,5-Bis(bromomethyl)benzoate (5): Methyl 3,5-dimethylbenzoate (6.00 g, 36.5 mmol) and NBS (13.80 g, 77.5 mmol) were suspended in CCl_4 (75 mL). The mixture was heated before AIBN was added in small portions while the flask was kept at reflux for 4 h. The white precipitate (succinimide) was filtered off. The residue was evaporated to dryness and recrystallized from EtOAc/hexane (8 mL/80 mL) while stored overnight in a fridge to give 4.80 g (41%) of white microcrystals. R_f = 0.67 (CH_2Cl_2); m.p. 93.9–94.1 °C (ref.[32] 95–97 °C). ^1H NMR (400 MHz, $CDCl_3$): δ = 3.93 (s, 3 H), 4.50 (s, 4 H), 7.62 (br. t, J = 1.7 Hz, 1 H), 8.00 (d, J = 1.7 Hz, 2 H) ppm. ^{13}C NMR (400 MHz, $CDCl_3$): δ = 165.9, 138.9, 133.8, 131.4, 130.0, 52.3, 31.8 ppm. HRMS (ESI): calcd. for $C_{10}H_{10}Br_2O_2$ $[M + H]^+$ 322.9100; found 322.9095; Δ = 1.5 ppm.

Methyl 3,5-Diformyl-4-hydroxybenzoate (6): Methyl 4-hydroxybenzoate (10.21 g, 66.4 mmol, 100 mol-%) and hexamethylenetetramine (38.37 g, 273.7 mmol, 412 mol-%) were dissolved in anhydrous THF (70 mL) and the yellow solution was heated at reflux for 4 d. Water (400 mL) was added to the viscous dark-orange solution and the mixture was heated up to give a homogeneous solution. After cooling, the product (12.09 g, 87%) was precipitated slowly (3 h) from solution. R_f = 0.88 (10:1 CH_2Cl_2/MeOH); m.p. 118–119 °C. ^1H NMR (400 MHz, $CDCl_3$): δ = 3.96 (s, 3 H), 8.65 (s, 2 H), 10.28 (s, 2 H), 12.05 (br. s, 1 H) ppm. ^{13}C NMR (400 MHz, $CDCl_3$): δ = 166.3, 164.8, 122.6, 120.8, 118.8, 52.6 ppm. HRMS (ESI): calcd. for $C_{10}H_9O_5$ $[M + H]^+$ 209.0450; found 209.0439; Δ = 5.3 ppm.

Methyl 4-Hydroxy-3,5-bis(hydroxymethyl)benzoate (7): Benzoate **6** (1.70 g, 8.2 mmol, 100 mol-%) was dissolved in MeOH (100 mL) and $NaBH_4$ (0.35 g, 9.3 mmol, 113 mol-%) was added at 0 °C. After stirring for 35 min, water (10 mL) was added and the solution

was concentrated in vacuo. The residue was made acidic (pH 2) by adding 1 M HCl and extracted with EtOAc (3 × 100 mL). The organic phase was washed with brine (3 × 100 mL) and dried (Na_2SO_4). The solvent was evaporated to give the product (1.41 g, 81%) as a yellow solid. R_f = 0.48 (10:1 CH_2Cl_2/MeOH); m.p. 117–118 °C. ^{1}H NMR (400 MHz, CD_3OD): δ = 3.85 (s, 3 H), 4.73 (s, 4 H), 7.86 (s, 2 H) ppm. ^{13}C NMR (400 MHz, CD_3OD): δ = 168.7, 159.3, 129.7, 128.4, 122.2, 61.6, 52.3 ppm. HRMS (ESI): calcd. for $C_{10}H_{13}O_5$ [M + H]$^+$ 213.0763; found 213.0732; Δ = 14.5 ppm.

Methyl 3,5-Bis(chloromethyl)-4-hydroxybenzoate (8): A solution of benzoate **7** (1.17 g, 5.5 mmol, 100 mol-%) and $SOCl_2$ (5 mL) was stirred under argon at room temp. for 3.5 h. Excess $SOCl_2$ was evaporated and the residue was diluted with $CHCl_3$ (40 mL) and washed with water (3 × 40 mL) and brine (3 × 40 mL). The solvent was removed to give the product (1.17 g, 85%) as light-yellow crystals. R_f = 0.37 (10:1 CH_2Cl_2/MeOH); m.p. 142–144 °C. ^{1}H NMR (400 MHz, $CDCl_3$): δ = 3.91 (s, 3 H), 4.71 (s, 4 H), 6.26 (br. s, 1 H), 8.01 (s, 2 H) ppm. ^{13}C NMR (400 MHz, $CDCl_3$): δ = 165.9, 157.2, 132.7, 124.6, 123.0, 52.2, 41.8 ppm. HRMS (ESI): calcd. for $C_{10}H_{11}Cl_2O_3$ [M + H]$^+$ 249.0085; found 249.0101; Δ = 6.4 ppm.

(6-Nitro-4*H*-benzo[*d*][1,3]dioxin-8-yl)methyl Acetate (9): 4-Nitrophenol (6.98 g, 50 mmol, 100 mol-%) was added to a mixture of paraformaldehyde (95%, 6.36 g, 201 mmol, 402 mol-%), acetic acid (25 mL), and sulfuric acid (11 mL) at 55 °C. After 5 min, a yellow precipitate formed. The mixture was cooled to room temp., acetic acid (10 mL) was added and heating was continued (60 °C). After heating at reflux for 22 h, the mixture was cooled to room temp. and water (50 mL) was added. The mixture was neutralized with solid K_2CO_3 (0.28 g, 203 mmol, 406 mol-%) and the grey-white solid was filtered and washed with cold water. The product was recrystallized from ethanol to give 7.09 g (56%) of **9** as a grey-white solid. R_f = 0.77 (10:1 CH_2Cl_2/MeOH); m.p. 115–116 °C (ref.[27] 118 °C). ^{1}H NMR (400 MHz, $CDCl_3$): δ = 2.08 (s, 3 H), 4.88 (s, 2 H), 5.07 (s, 2 H), 5.29 (s, 2 H), 7.81 (d, J = 2.6 Hz, 1 H), 8.05 (d, J = 2.8 Hz, 1 H) ppm. ^{13}C NMR (400 MHz, $CDCl_3$): δ = 170.5, 155.2, 141.2, 125.3, 123.2, 121.2, 121.0, 91.9, 65.9, 59.8, 20.8 ppm.

2,6-Bis(bromomethyl)-4-nitrophenol (10): Dioxine **9** (2.02 g, 8.0 mmol, 100 mol-%) was dissolved in HBr (48%, 60 mL) and the mixture was heated at reflux for 16 h. The mixture was then cooled to room temp. and the solid was filtered and washed with cold water. The crude product was recrystallized from chloroform, dried with THF, and recrystallized from EtOH/hexane to give 2.17 g (86%) of a grey-white product. R_f = 0.24 (10:1 CH_2Cl_2/MeOH); m.p. 149–150 °C (ref.[27] 146–147 °C). ^{1}H NMR (400 MHz, $CDCl_3$): δ = 4.57 (s, 4 H), 6.41 (br. s, 1 H), 8.22 (s, 2 H) ppm. ^{13}C NMR (400 MHz, $CDCl_3$): δ = 158.3, 141.0, 126.6, 125.7, 27.1 ppm.

2,6-Dimethylanisole (11): 2,6-Dimethylphenol (8.00 g, 65.5 mmol, 100 mol-%) was dissolved in acetone (100 mL) and MeI (28.0 g, 200 mmol, 305 mol-%) and K_2CO_3 (18.5 g, 134 mmol, 204 mol-%) were added to the solution. The reaction mixture was heated at reflux for 3 d and then the solvent was evaporated in vacuo. The residue was dissolved in EtOAc (100 mL), washed with saturated $NaHCO_3$ (3 × 100 mL) and brine (3 × 100 mL), and dried (Na_2SO_4). The solvent was evaporated to give 7.75 g (87%) of the product. R_f = 0.52 (10:1 cyclohexane/EtOAc). ^{1}H NMR (400 MHz, $CDCl_3$): δ = 2.28 (s, 6 H), 3.72 (s, 3 H), 6.91 (t, J = 7.4 Hz, 1 H), 7.00 (d, J = 7.7 Hz, 2 H) ppm. ^{13}C NMR (400 MHz, $CDCl_3$): δ = 157.0, 130.8, 128.8, 123.7, 59.6, 16.0 ppm.

2,6-Bis(bromomethyl)anisole (12): A few crystals of AIBN were added to a solution of 2,6-dimethylanisole (3.07 g, 22.5 mmol, 100 mol-%) and *N*-bromosuccinimide (8.24 g, 46.4 mmol, 206 mol-%) in CCl_4 (30 mL). The mixture was heated to 85 °C and more AIBN was added. After heating at reflux (2 h) the color of the solution changed rapidly from yellow to white and the mixture was cooled to room temp. The solid was removed by filtration and the solution was concentrated in vacuo. The crude product was recrystallized from EtOAc/hexane to give 2.86 g (43%) of light-yellow crystals. R_f = 0.78 (30:1 CH_2Cl_2/MeOH); m.p. 85.4–85.6 °C (ref.[33] 83–85 °C). ^{1}H NMR (400 MHz, $CDCl_3$): δ = 4.03 (s, 3 H), 4.56 (s, 4 H), 7.12 (t, J = 7.6 Hz, 1 H), 7.38 (d, J = 7.7 Hz, 2 H) ppm. ^{13}C NMR (400 MHz, $CDCl_3$): δ = 156.6, 132.2, 131.9, 125.0, 62.2, 29.5 ppm.

2,6-Bis(bromomethyl)phenol (13): Boron tribromide (1.1 M CH_2Cl_2, 7.0 mL, 7.7 mmol, 151 mol-%) was added to anisole **12** (1.50 g, 5.1 mmol, 100 mol-%) at –78 °C. Stirring was continued at room temp. for 3 h. The reaction was quenched with water (8 mL) and diluted with EtOAc (40 mL). The organic phase was washed with brine (2 × 20 mL) and dried (Na_2SO_4). The solvent was evaporated to give the product (1.27 g, 89%) as a yellow solid. R_f = 0.69 (30:1 CH_2Cl_2/MeOH); m.p. 101–102 °C (ref.[34] 80–82 °C). ^{1}H NMR (400 MHz, $CDCl_3$): δ = 4.57 (s, 4 H), 6.90 (t, J = 7.6 Hz, 1 H), 7.27 (d, J = 7.7 Hz, 2 H) ppm. ^{13}C NMR (400 MHz, $CDCl_3$): δ = 153.4, 131.4, 125.2, 121.2, 29.3 ppm.

Synthesis of Chelate Methyl 4-[Bis(pyridin-2-ylmethyl)aminomethyl]benzoate (2a). Typical Procedure: A mixture of *p*-(halomethyl)-benzoate **4** (2.29 g, 10.0 mmol, 100 mol-%), Dpa (2.05 mL, 11.0 mmol, 110 mol-%), K_2CO_3 (1.45 g, 10.5 mmol, 105 mol-%), and DMF (10.0 mL) was stirred under argon at room temp. for 24 h. After stirring, the solution was diluted with EtOAc (25 mL) and washed with water (3 × 25 mL) and saturated NaCl (3 × 25 mL). The organic phase was dried (Na_2SO_4) and concentrated in vacuo to give the pure product (2.16 g, 62%). R_f = 0.60 (10:1 CH_2Cl_2/MeOH). ^{1}H NMR (400 MHz, $CDCl_3$): δ = 3.75 (s, 2 H), 3.81 (s, 4 H), 3.90 (s, 3 H), 7.15 (ddd, J = 7.2, 5.0, 1.0 Hz, 2 H), 7.49 (d, J = 8.2 Hz, 2 H), 7.55 (d, J = 7.9 Hz, 2 H), 7.67 (dt, J = 7.7, 1.8 Hz, 2 H), 7.98 (dt, J = 8.2 Hz, 2 H), 8.52 (d, J = 5.0 Hz, 2 H) ppm. ^{13}C NMR (400 MHz, $CDCl_3$) δ = 167.0, 159.3, 149.0, 144.6, 136.4, 129.6, 128.7, 122.8, 122.0, 100.1, 60.0, 58.2, 52.0 ppm. HRMS (ESI): calcd. for $C_{21}H_{21}N_3NaO_2$ [M + Na]$^+$ 370.1531; found 370.1569; Δ = 10.3 ppm.[35]

Methyl 3,5-Bis[bis(pyridin-2-ylmethyl)aminomethyl]benzoate (2b): Yield 0.95 g (57%); R_f = 0.13 (10:1 CH_2Cl_2/MeOH). ^{1}H NMR (400 MHz, $CDCl_3$): δ = 3.74 (s, 4 H), 3.81 (s, 8 H), 3.92 (s, 3 H), 7.13 (ddd, J = 7.2, 5.0, 1.5 Hz, 4 H), 7.57 (d, J = 7.7 Hz, 4 H), 7.62 (dt, J = 7.7, 1.6 Hz, 4 H), 7.71 (br. t, J = 1.5 Hz, 1 H), 7.94 (d, J = 1.5 Hz, 2 H), 8.52 (dd, J = 5.0, 0.7 Hz, 4 H) ppm. ^{13}C NMR (400 MHz, $CDCl_3$): δ = 167.1, 159.5, 149.0, 139.8, 136.4, 133.8, 130.2, 128.7, 122.8, 122.0, 60.1, 58.2, 52.1 ppm. HRMS (ESI): calcd. for $C_{34}H_{35}N_6O_2$ [M + H]$^+$ 559.2821; found 559.2824; Δ = 0.5 ppm.

Methyl 3,5-Bis[bis(pyridin-2-ylmethyl)aminomethyl]-4-hydroxybenzoate (2c): Yield 1.06 g (80%); R_f = 0.61 (6:1 CH_2Cl_2/MeOH). ^{1}H NMR (400 MHz, $CDCl_3$): δ = 3.84 (s, 4 H), 3.88 (s, 3 H), 3.89 (s, 8 H), 7.13 (ddd, J = 7.3, 4.9, 1.1 Hz, 4 H), 7.49 (d, J = 7.9 Hz, 4 H), 7.61 (dt, J = 7.7, 1.8 Hz, 4 H), 7.95 (s, 2 H), 8.52 (dd, J = 4.9, 0.7 Hz, 4 H) ppm. ^{13}C NMR (400 MHz, CD_3OD): δ = 160.7, 159.1, 148.8, 136.6, 131.1, 124.4, 122.9, 122.0, 59.7, 54.5, 51.7 ppm. HRMS (ESI): calcd. for $C_{34}H_{34}N_6NaO_3$ [M + Na]$^+$ 597.2590; found 597.2610; Δ = 3.3 ppm.

2,6-Bis[bis(pyridin-2-ylmethyl)aminomethyl]-4-nitrophenol (2d): Yield 0.69 g (77%); R_f = 0.29 (10:1 CH_2Cl_2/MeOH). ^{1}H NMR (400 MHz, CD_3OD): δ = 3.84 (s, 4 H), 3.89 (s, 8 H), 7.24 (ddd, J = 7.5, 4.9, 1.1 Hz, 4 H), 7.53 (d, J = 7.9 Hz, 4 H), 7.71 (dt, J =

7.7, 1.8 Hz, 4 H), 8.06 (s, 2 H), 8.43 (dd, J = 5.1, 0.9 Hz, 4 H) ppm. ^{13}C NMR (400 MHz, $CDCl_3$): δ = 162.3, 158.6, 148.7, 139.4, 136.7, 125.3, 125.0, 122.8, 122.1, 59.6, 54.0 ppm. HRMS (ESI): calcd. for $C_{32}H_{31}N_7NaO_3$ $[M + Na]^+$ 584.2386; found 584.2368; Δ = 3.1 ppm.

2,6-Bis[bis(pyridin-2-ylmethyl)aminomethyl]phenol (2e): Yield 0.88 g (51%); R_f = 0.57 (10:1 CH_2Cl_2/MeOH). ^{1}H NMR (400 MHz, $CDCl_3$): δ = 3.83 (s, 4 H), 3.88 (s, 8 H), 6.78 (t, J = 7.5 Hz, 1 H), 7.11 (t, J = 6.0 Hz, 4 H), 7.23 (d, J = 7.5 Hz, 2 H), 7.50 (d, J = 7.8 Hz, 4 H), 7.59 (t, J = 7.6 Hz, 4 H), 8.52 (t, J = 4.3 Hz, 4 H) ppm. ^{13}C NMR (400 MHz, $CDCl_3$): δ = 159.1, 155.8, 148.7, 136.4, 129.0, 123.9, 122.8, 121.8, 118.3, 59.6, 54.5 ppm. HRMS (ESI): calcd. for $C_{32}H_{33}N_6O$ $[M + H]^+$ 517.2716; found 517.2715; Δ = 0.2 ppm.[18]

Supporting Information (see also the footnote on the first page of this article): Binding constant measurements for chelates **2b**–**e**, ^{1}H and ^{13}C NMR spectra of compounds **2a**–**e**, Cartesian coordinates for the geometry-optimized zinc imidazole chelate structures **2b**–**e** (Table 3).

Acknowledgments

Prof. Craig S. Wilcox, University of Pittsburgh, is gratefully acknowledged for his advice on the chelate titration protocol. This work was financially supported by the Finnish National Technology Agency (TEKES) and EU COST action D28. T. R. also thanks the Gustaf Komppa Fund of the Alfred Kordelin Foundation.

[1] D. P. Beer, A. P. Gale, *Angew. Chem. Int. Ed.* **2001**, *40*, 486–516.
[2] D. P. Beer, S. R. Bayly, *Top. Curr. Chem.* **2005**, *255*, 125–162.
[3] B. Linton, A. D. Hamilton, *Chem. Rev.* **1997**, *97*, 1669–1680.
[4] G. Parkin, *Chem. Rev.* **2004**, *104*, 699–767.
[5] R. W. Strange, S. Antonyuk, M. A. Hough, P. A. Doucette, J. A. Rodriguez, P. J. Hart, L. J. Hayward, J. S. Valentine, S. S. Hasnain, *J. Mol. Biol.* **2003**, *328*, 877–891.
[6] a) H. Ohtsu, S. Itoh, S. Nagatomo, T. Kitagawa, S. Ogo, Y. Watanabe, S. Fukuzumi, *Inorg. Chem.* **2001**, *40*, 3200–3207; b) D. Li, S. Li, D. Yang, J. Yu, J. Huang, Y. Li, W. Tang, *Inorg. Chem.* **2003**, *42*, 6071–6080, and references cited therein.
[7] E. J. O'Neil, B. D. Smith, *Coord. Chem. Rev.* **2006**, *250*, 3068–3080.
[8] R. G. Lacoste, A. E. Martell, *Inorg. Chem.* **1964**, *3*, 881–884.
[9] J. K. Romary, J. D. Barger, J. E. Bunds, *Inorg. Chem.* **1968**, *6*, 1142–1145.
[10] More than 1000 Dpa–transition-metal chelate structures can be found in the Cambridge Crystal Structure Database. The most abundant metals are Cu, Fe, Zn, Mn, Ni, Co, Rh and Ru in decreasing order.
[11] J. Wirbser, H. Vahrenkamp, *Z. Naturforsch., Teil B* **1992**, *47*, 962–968.
[12] Y. Gultneh, A. R. Khan, D. Blaise, S. Chaudhry, B. Ahvazi, B. B. Marvey, R. J. Butcher, *J. Inorg. Biochem.* **1999**, *75*, 7–18.
[13] a) A. Mokhir, R. Krämer, H. Wolf, *J. Am. Chem. Soc.* **2004**, *126*, 6208–6209; b) P. Jiang, Z. Guo, *Coord. Chem. Rev.* **2004**, *248*, 205–229.
[14] G. K. Walkup, S. C. Burdette, S. J. Lippard, R. Y. Tsien, *J. Am. Chem. Soc.* **2000**, *122*, 5644–5645.
[15] N. C. Lim, C. Brückner, *Chem. Commun.* **2004**, *9*, 1094–1095.
[16] C. J. Chang, E. M. Nolan, J. Jaworski, S. C. Burdette, M. Sheng, S. J. Lippard, *Chem. Biol.* **2004**, *11*, 203–210.
[17] a) A. Ojida, Y. Mito-oka, K. Sada, I. Hamachi, *J. Am. Chem. Soc.* **2004**, *126*, 2454–2463; b) A. Ojida, M. Inoue, Y. Mito-oka, I. Hamachi, *J. Am. Chem. Soc.* **2003**, *125*, 10184–10185; c) A. Ojida, Y. Mito-oka, M. Inoue, I. Hamachi, *J. Am. Chem. Soc.* **2002**, *124*, 6256–6258.
[18] a) D. H. Lee, S. Y. Kim, J.-I. Hong, *Angew. Chem. Int. Ed.* **2004**, *43*, 4777–4780; b) D. H. Lee, J. H. Im, S. U. Son, Y. K. Chung, J.-I. Hong, *J. Am. Chem. Soc.* **2003**, *125*, 7752–7753.
[19] H. Jiang, E. J. O'Neil, K. M. DiVittorio, B. D. Smith, *Org. Lett.* **2005**, *7*, 3013–3016.
[20] Y. Mito-oka, S. Tsukiji, T. Hiraoka, N. Kasagi, S. Shinkai, I. Hamachi, *Tetrahedron Lett.* **2001**, *42*, 7059–7062.
[21] a) L. Fabbrizzi, G. Francese, M. Licchelli, A. Perotti, A. Taglietti, *Chem. Commun.* **1997**, 581–582; b) M. A. Hortala, L. Fabbrizzi, N. Marcotte, F. Stomeo, A. Taglietti, *J. Am. Chem. Soc.* **2003**, *125*, 20–21.
[22] a) P. Dapporto, M. Formica, V. Fusi, L. Giorgi, M. Micheloni, P. Paoli, R. Pontellini, P. Rossi, *Inorg. Chem.* **2001**, *40*, 6186–6192; b) P. Dapporto, M. Formica, V. Fusi, M. Micheloni, P. Paoli, R. Pontellini, P. Rossi, *Inorg. Chem.* **2000**, *39*, 4663–4665.
[23] H. Togo, T. Hirai, *Synlett* **2003**, *5*, 702–704.
[24] L. F. Lindoy, G. V. Meehan, N. Svenstrup, *Synthesis* **1998**, 1029–1032.
[25] C. Pulgarin, J. Gunzinger, R. Tabacchi, *Helv. Chim. Acta* **1985**, *68*, 1948–1951.
[26] S. M. Dimick, S. C. Powell, S. A. McMahon, D. N. Moothoo, J. H. Naismith, E. J. Toone, *J. Am. Chem. Soc.* **1999**, *121*, 10286–10296.
[27] J. de Mendoza, P. M. Nieto, P. Prados, C. Sánchez, *Tetrahedron* **1990**, *46*, 671–682.
[28] C. S. Wilcox in *Frontiers in Supramolecular Organic Chemistry and Photochemistry* (Eds.: H. J. Schneider, H. Dürr), VCH, Weinheim, **1991**, pp. 123–143.
[29] At least two equilibria contribute to the imidazole binding (mono vs. bidentate).
[30] H. Günther, *The Influence of Dynamic Effects on NMR Spectra*, 2nd ed., Wiley, Chichester, **1995**, chapter 9.
[31] R. C. Fuson, H. G. Cooke, *J. Am. Chem. Soc.* **1940**, *62*, 1180–1183.
[32] P. Liu, Y. Chen, J. Deng, Y. Tu, *Synthesis* **2001**, *14*, 2078–2080.
[33] M. Ashram, D. O. Miller, J. N. Bridson, P. E. Georgiou, *J. Org. Chem.* **1997**, *62*, 6476–6484.
[34] J. C. Rosa, D. Galanakis, A. Piergentili, K. Bhandari, C. R. Ganellin, P. M. Dunn, D. H. Jenkinson, *J. Med. Chem.* **2000**, *43*, 420–431.
[35] D. R. van Staveren, E. Bothe, T. Weyhermüller, N. Metzler-Nolte, *Eur. J. Inorg. Chem.* **2002**, *6*, 1518–1529.

Received: September 28, 2007
Published Online: May 6, 2008

